Phagocytosis and conidiocidal assays

Alveolar macrophages were exposed to conidia at a macrophage:conidia ratio of 1:5 for 2 h, and 10:1 for 4 h, in the absence or presence of 20 $\mu g\,ml^{-1}$ Ptx3 (0.44×10^{-6} M Ptx3 protomer) before being evaluated for internalization or conidiocidal activity, respectively (Supplementary Information).

Received 26 July; accepted 8 October 2002; doi:10.1038/nature01195.

1. Emsley, J. *et al.* Structure of pentameric human serum amyloid P component. *Nature* **367,** 338–345 (1994).
2. Szalai, A. J., Agrawal, A., Greenhough, T. J. & Volanakis, J. E. C-reactive protein structural biology, gene expression, and host defense function. *Immunol. Res.* **16,** 127–136 (1997).
3. Steel, D. M. & Whitehead, A. S. The major acute phase reactants: C-reactive protein: serum amyloid P component and serum amyloid A protein. *Immunol. Today* **15,** 81–88 (1994).
4. Pepys, M. B. & Baltz, M. L. Acute phase proteins with special reference to C-reactive protein and related proteins (pentaxins) and serum amyloid A protein. *Adv. Immunol.* **34,** 141–212 (1983).
5. Noursadeghi, M. *et al.* Role of serum amyloid P component in bacterial infection: protection of the host or protection of the pathogen. *Proc. Natl Acad. Sci. USA* **97,** 14584–14589 (2000).
6. Mantovani, A., Garlanda, C. & Bottazzi, B. *Cytokine Reference* (eds Oppenheim, J. & Feldmann, M.) (Academic, New York, 2002).
7. Breviario, F. *et al.* Interleukin-1-inducible genes in endothelial cells. Cloning of a new gene related to C-reactive protein and serum amyloid P component. *J. Biol. Chem.* **267,** 22190–22197 (1992).
8. Lee, G. W., Lee, T. H. & Vilcek, J. TSG-14, a tumour necrosis factor- and IL-1-inducible protein, is a novel member of the pentaxin family of acute phase proteins. *J. Immunol.* **150,** 1804–1812 (1993).
9. Vidal Alles, V. *et al.* Inducible expression of PTX3, a new member of the pentraxin family, in human mononuclear phagocytes. *Blood* **84,** 3483–3493 (1994).
10. Introna, M. *et al.* Cloning of mouse PTX3, a new member of the pentraxin gene family expressed at extrahepatic sites. *Blood* **87,** 1862–1872 (1996).
11. Bottazzi, B. *et al.* Multimer formation and ligand recognition by the long pentraxin PTX3 – similarities and differences with the short pentraxins C-reactive protein and serum amyloid P component. *J. Biol. Chem.* **272,** 32817–32823 (1997).
12. Rovere, P. *et al.* The long pentraxin PTX3 binds to apoptotic cells and regulates their clearance by antigen-presenting dendritic cells. *Blood* **96,** 4300–4306 (2000).
13. Lee, G. W., Goodman, A. R., Lee, T. H. & Vilcek, J. Relationship of TSG-14 protein to the pentraxin family of major acute phase proteins. *J. Immunol.* **153,** 3700–3707 (1994).
14. Varani, S. *et al.* Knockout of pentraxin 3, a downstream target of growth differentiation factor-9, causes female subfertility. *Mol. Endocrinol.* **16,** 1154–1167 (2002).
15. Medzhitov, R. Toll-like receptors and innate immunity. *Nature Rev. Immunol.* **1,** 135–145 (2001).
16. Denning, D. W. Invasive aspergillosis. *Clin. Infect. Dis.* **26,** 781–803 (1998).
17. Cenci, E. *et al.* Th1 and Th2 cytokines in mice with invasive aspergillosis. *Infect. Immun.* **65,** 564–570 (1997).
18. Mencacci, A. *et al.* Defective antifungal T-helper 1 (TH1) immunity in a murine model of allogeneic T-cell-depleted bone marrow transplantation and its restoration by treatment with TH2 cytokine antagonists. *Blood* **97,** 1483–1490 (2001).
19. Schaffner, A., Douglas, H. & Braude, A. Selective protection against conidia by mononuclear and against mycelia by polymorphonuclear phagocytes in resistance to *Aspergillus*. Observations on these two lines of defense *in vivo* and *in vitro* with human and mouse phagocytes. *J. Clin. Invest.* **69,** 617–631 (1982).
20. Romani, L. The T cell response against fungal infections. *Curr. Opin. Immunol.* **9,** 484–490 (1997).
21. Mencacci, A. *et al.* Cytokines in candidiasis and aspergillosis. *Curr. Pharm. Biotechnol.* **1,** 235–251 (2000).
22. Bozza, S. *et al.* Dendritic cells transport conidia and hyphae of *Aspergillus fumigatus* from the airways to the draining lymph nodes and initiate disparate Th responses to the fungus. *J. Immunol.* **168,** 1362–1371 (2002).
23. Botto, M. *et al.* Homozygous C1q deficiency causes glomerulonephritis associated with multiple apoptotic bodies. *Nature Genet.* **19,** 56–59 (1998).
24. Peri, G. *et al.* PTX3, a prototypic long pentraxin, is an early indicator of acute myocardial infarction in man. *Circulation* **102,** 636–641 (2000).
25. Muller, B. *et al.* Circulating levels of the long pentraxin PTX3 correlate with severity of infection in critically ill patients. *Crit. Care Med.* **29,** 1404–1407 (2001).
26. Villa, P. *et al.* Pattern of cytokines and pharmacomodulation in sepsis induced by cecal ligation and puncture compared with that induced by endotoxin. *Clin. Diagn. Lab. Immunol.* **2,** 549–553 (1995).
27. Watanabe, Y., Mitsuyama, M., Sano, M., Nakano, H. & Nomoto, K. Enhanced resistance against *Listeria monocytogenes* at an early phase of primary infection in pregnant mice: activation of macrophages during pregnancy. *Infect. Immun.* **52,** 730–735 (1986).

Supplementary Information accompanies the paper on *Nature*'s website (http://www.nature.com/nature).

Acknowledgements This work was supported by Istituto Superiore di Sanità, Ministero Istruzione, Università e Ricerca (MIUR), Consiglio Nazionale della Richerche (CNR), and by the European Commission. We acknowledge the contribution of the Italian Association for Cancer Research. We thank C. Scotton for critical reading of the manuscript.

Competing interests statement The authors declare competing financial interests: details accompany the paper on *Nature*'s website (http://www.nature.com/nature).

Correspondence and requests for materials should be addressed to A.M. (e-mail: mantovani@marionegri.it).

Escherichia coli K-12 undergoes adaptive evolution to achieve *in silico* predicted optimal growth

Rafael U. Ibarra*†, Jeremy S. Edwards†‡ & Bernhard O. Palsson*

* *Department of Bioengineering, University of California, San Diego, 9500 Gilman Drive, La Jolla, California 92093-0412, USA*
‡ *Department of Chemical Engineering, University of Delaware, Newark, Delaware 19716, USA*
† *These authors contributed equally to this work*

Annotated genome sequences[1,2] can be used to reconstruct whole-cell metabolic networks[3–6]. These metabolic networks can be modelled and analysed (computed) to study complex biological functions[7–11]. In particular, constraints-based *in silico* models[12] have been used to calculate optimal growth rates on common carbon substrates, and the results were found to be consistent with experimental data under many but not all conditions[13,14]. Optimal biological functions are acquired through an evolutionary process. Thus, incorrect predictions of *in silico* models based on optimal performance criteria may be due to incomplete adaptive evolution under the conditions examined. *Escherichia coli* K-12 MG1655 grows sub-optimally on glycerol as the sole carbon source. Here we show that when placed under growth selection pressure, the growth rate of *E. coli* on glycerol reproducibly evolved over 40 days, or about 700 generations, from a sub-optimal value to the optimal growth rate predicted from a whole-cell *in silico* model. These results open the possibility of using adaptive evolution of entire metabolic networks to realize metabolic states that have been determined a priori based on *in silico* analysis.

Predictive whole-cell metabolic models can be developed using a constraints-based modelling procedure[15–18]. As an alternative to detailed theory-based models, constraints-based models use the successive imposition of governing constraints (such as mass conservation, thermodynamics, capacity and nutritional environment) to eliminate network functions that exceed the governing constraints. Mathematically this procedure defines a solution space containing all possible metabolic network functions that satisfy the governing constraints. Each particular solution in this space corresponds to a particular state of the metabolic network and therefore a potential behaviour of the cell. Within the solution space defined by the governing constraints, the optimal use of the metabolic network to support growth can be found among all possible solutions using linear optimization[16–19]. However, a single optimal growth condition is of limited interest and a phenotype phase plane (PPP) analysis has been developed to obtain a broad understanding of a metabolic network's optimal properties[20,21]. The PPP analysis evaluates the optimal properties of a metabolic network under a range of environmental conditions (see Methods) and has been used to show that the growth of *E. coli* is consistent with the optimal use of its metabolic network under several defined growth conditions[12–14].

It is not known whether optimal growth is observed on all substrates, and if not, whether adaptive evolution towards optimal growth can be achieved. Furthermore, if such adaptive evolution towards the optimal behaviour occurs, does the endpoint correspond with a priori calculations? To address these issues, we examined prolonged exponential growth of *E. coli* K-12 on several substrates (acetate, succinate, malate, glucose and glycerol). All calculations presented here were made with a previously formulated large-scale *E. coli* metabolic model[12,14], and the model was not adjusted or 'fitted' to the data described.

Batch growth experiments were done using malate as the sole

carbon source with a range of substrate concentrations (0.25–3 g l^{-1}) and temperatures (29–37 °C) to vary the malate uptake rate (MUR). The MUR, oxygen uptake rate (OUR) and growth rate were measured. The measured MUR and OUR data were optimal, as defined by the line of optimality (LO) in the PPP (Fig. 1a). The optimal growth rate of *E. coli* was calculated for all combinations of the MUR and OUR and displayed as a surface over the PPP (Fig. 1b). The experimentally determined growth rates were on the edge of the colour-coded solution space that corresponds to the LO (Fig. 1b). Hence the optimal growth performance of *E. coli* K-12 on malate was predicted *a priori* by using PPP. The results for growth with malate as the sole carbon source were in agreement with previous observations of *E. coli* metabolism for growth on succinate or acetate[14].

A natural question arises: is the optimal performance on malate stable over prolonged periods of time? To address this question, adaptive evolution of *E. coli* on malate was studied for 500 generations. The adaptation resulted in a 19% increase in growth rate. However, the MUR and OUR also increased and maintained metabolic operation on the LO (Fig. 1). Similar adaptive evolution experiments on acetate and succinate resulted in an increased growth rate (20% and 17%, respectively) (Fig. 2). Both the oxygen and substrate uptake rates increased concomitantly to maintain optimal growth as defined and predicted by the PPP analysis.

The growth rate of *E. coli* using glucose as the carbon source was also increased by prolonged exponential growth (Figs 2 and 3). Before adaptive evolution on glucose the cellular growth rate, OUR, and glucose uptake rate (GUR) were experimentally determined over a range of glucose concentrations and temperatures. The experimentally determined values for the GUR and OUR corresponded to points on the LO or slightly in phase 2 (the acetate overflow region) of the PPP (ref. 21) (Fig. 3a). The predicted acetate secretion in phase 2 was experimentally observed and the measured growth rates were on the surface of the solution space near the edge corresponding to the LO (data not shown). *E. coli* was subsequently kept in sustained exponential growth over 500 generations (Fig. 3b, c). The growth rate increased by 17%, as shown by movement of the experimental data points within phase 2 on the surface towards higher growth rates. Thus, as with malate, succinate and acetate, the growth rate of *E. coli* with glucose as the carbon source could be slightly increased with the substrate and oxygen uptake rates moving in phase 2 with some acetate overflow. It was also noted that evolutionary adaptation maintained metabolic operation on the surface of the three-dimensional PPP, as predicted by the physicochemical constraints on the metabolic network. The metabolic operation in the phase 2 provided an increased growth rate with a reduced yield (relative to the LO).

We determined the growth performance over a range of glycerol concentrations and temperature. Unlike growth on malate or glucose, the experimental data points were scattered throughout phase 1 far from the LO (Fig. 4b), indicating sub-optimal growth of

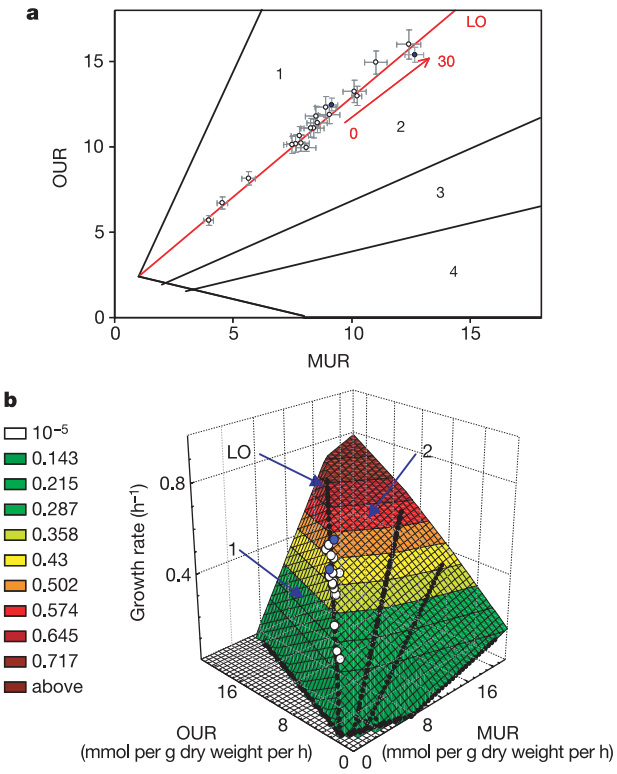

Figure 1 Growth of *E. coli* K-12 on malate. **a**, The malate–oxygen phenotype phase plane (PPP) Phase 1 is characterized by metabolic futile cycles, whereas phase 2 is characterized by acetate overflow metabolism. The line of optimality (LO, in red) separates phases 1 and 2 (ref. 21.) Data points (open circles) represent malate concentrations ranging from 0.25–3 g l^{-1}; and temperatures ranging from 29–37 °C. The two data points in blue represent the starting point (day 0) and endpoint (day 30) of adaptive evolution respectively, at a malate concentration of 2 g l^{-1} and a temperature of 37 °C. These data points represent a span of 500 generations. **b**, Three-dimensional representation of growth rates. The *x* and *y* axes represent the same variables as in **a**. The *z* axis represents the cellular growth rate (h^{-1}). OUR, oxygen uptake rate; MUR, malate uptake rate.

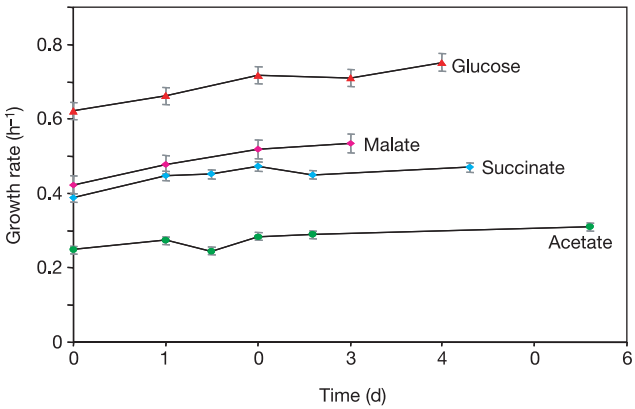

Figure 2 Growth rate during adaptive evolution on glucose, malate, succinate and acetate. Growth conditions were kept constant at a temperature of 37 °C and a substrate concentration of 2 g l^{-1}. We measured growth rate in the exponential phase of growth. The increases in growth rate over time were as follows: glucose (18%), malate (21%), succinate (17%) and acetate (20%). The number of generations for each adaptive evolution was: glucose (500), malate (500), succinate (1,000) and acetate (700).

wild-type *E. coli* K-12 on glycerol, consistent with previous observations[22].

We studied *E. coli* adaptive growth using glycerol as the sole carbon source (2 g l^{-1}), by serial transfer, at a temperature of 30 °C, and with sufficient oxygenation. Growth rate, glycerol uptake rate (G1-UR) and OUR were measured every ten days. Over a 40-day period an evolutionary path (E1) was observed (Fig. 4c). Phenotypic changes were traced in phase 1, eventually converging towards the LO. During this 40-day period, the growth rate more than doubled from 0.23 h^{-1} to 0.55 h^{-1} (Fig. 4a). The substrate uptake and growth rate data obtained under various growth conditions after adaptive evolution were near the LO (Fig. 4d). The evolved strain attained near-optimal growth on glycerol as defined by the *in silico* predictions. A second, independent adaptation experiment gave a similar but non-identical evolutionary trajectory (E2), converging near the same endpoint (Fig. 4c). Finally, a third independent adaptation experiment (E3) was done with a different initial starting point within phase 1. E3 was done at 37 °C and a glycerol concentration of 2 g l^{-1}. The adaptation of *E. coli* to growth on glycerol at 37 °C resulted in motion towards the LO and the growth rate increased by about 30% (Fig. 4a). The final growth rate of the E3 strain was consistent with the *in silico* predictions with respect to the G1-UR, OUR and the growth rate.

To assess the stability of the endpoint of the adaptive evolution, we extended the cultivation on glycerol for an additional 300 generations, or 20 days for the E1 and E2 strains. The data indicated no further change in growth (Fig. 4a). On the sixtieth day of the experiment the E1 and E2 strains exhibited growth on the LO under various growth conditions, reaffirming optimal growth behaviour and the stability of the phenotype (Fig. 4e).

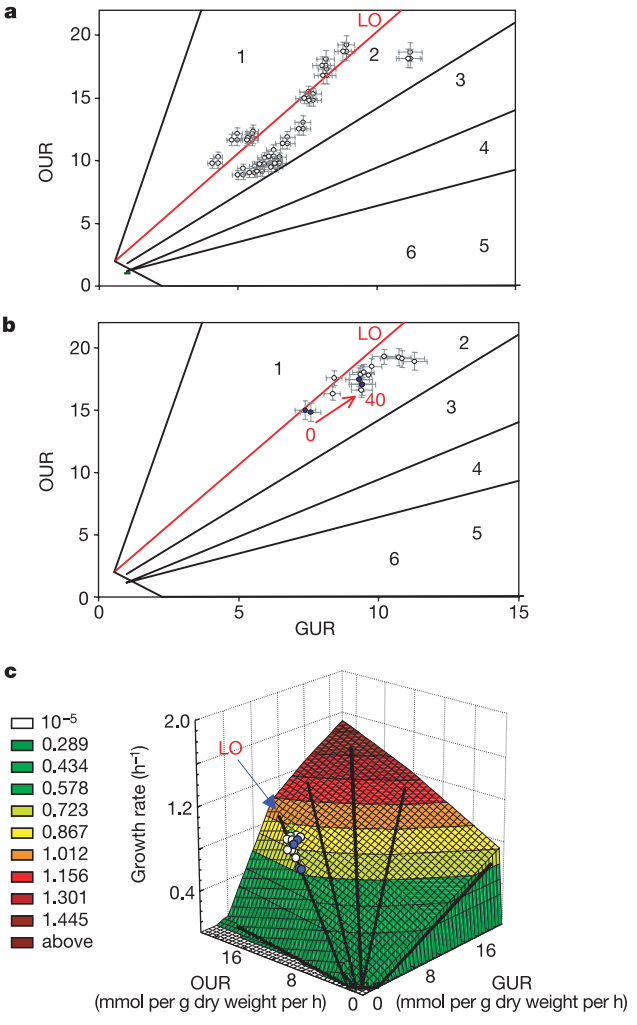

Figure 3 Growth of *E. coli* K-12 on glucose. **a**, The glucose–oxygen PPP. Like the malate–oxygen PPP, phase 1 represents sub-optimal growth and phase 2 is characterized by acetate overflow metabolism. The LO is shown in red. **b**, GUR plotted against OUR along with experimental values for adaptive evolution experiments. Open circles represent measurements during the adaptive evolutionary process, whereas blue circles indicate the beginning and end of evolution. **c**, Three-dimensional rendering of computed growth rate and the experimental data (from **a** and **b**). The *x* and *y* axes represent the GUR and OUR. The *z* axis represents the cellular growth rate (h^{-1}).

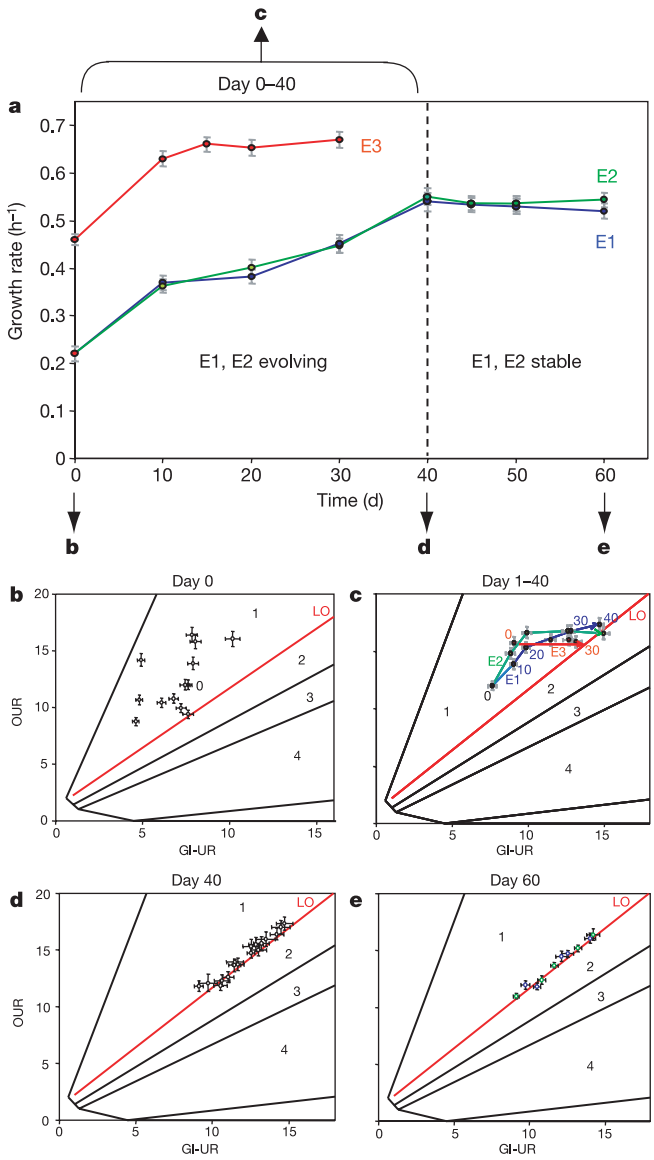

Figure 4 Growth of *E. coli* K-12 on glycerol. **a**, Change in growth rate with time for three adaptive evolution experiments: trajectories E1, E2, and E3. E1 and E2 were performed at 30 °C and E3 at 37 °C. The glycerol concentration was kept constant at 2 g l^{-1} during E1, E2 and E3. **b**, The PPP pre-evolution. The LO is shown in red. The range of glycerol concentrations used was 0.25–2 g l^{-1}. **c**, The PPP during adaptive evolution. Experimental values for E1 are indicated in blue, and for E2 they are indicated in green, and for E3 in red. The starting point of evolution for E1 and E2 is indicated in black (day 0). **d**, The PPP after 40 days (about 700 generations) of evolution. The range of glycerol concentrations used was 0.25–2 g l^{-1}. **e**, The PPP after 60 days (1,000 generations) of evolution. The range of glycerol concentrations used was 0.25–2 g l^{-1}. Data points were obtained using the E1 (blue) and E2 (green) strains. GI-UR, glycerol uptake rate.

Selection pressure is expected to result in optimal performance through an evolutionary process. Optimal growth of *E. coli* on acetate, succinate, malate and glucose is consistent with the predictions of whole-cell *in silico* models. The strain used here has presumably never had to compete for survival using glycerol as the sole carbon source and thus initially utilized this carbon source non-optimally. However, adaptive evolution on glycerol resulted in the a priori calculated optimal growth that was based on the constraints placed on the *E. coli* metabolic network. The adaptive evolutionary process had a reproducible and predictable endpoint.

This study opens up several possibilities. First, it may now be possible to specify optimal network properties *in silico* and achieve them through an adaptive evolutionary process or in combination with a series of other methodologies. *In silico* design of microorganisms could be used to improve their metabolic abilities, production efficiency and/or operational longevity. Second, changes in mRNA expression levels and DNA sequences can now be monitored as cells progress along a defined evolutionary path. Such experiments may yield valuable insight into the molecular design of complex control circuits and their adaptation during evolution. The combination of *in silico* and experimental biology introduced here may make a new series of biological designs attainable.

Constraint-based computational models use an optimization-based procedure to predict cellular states. It is assumed that this optimal state, within the governing constraints, is found by altering the numerical values of the kinetic and regulatory constants through a 'trial-and-error' process. This feature of constraint-based models is a significant departure from other types of mathematical models of cell function, where these parameters are treated as being time-invariant. Thus constraint-based models directly account for the fundamental nature of adaptive evolution. The adaptive evolutionary path itself cannot be predicted; however, the final outcome can be. □

Methods

Strains and media

The *E. coli* K-12 MG1655 annotated genome sequence and the biochemical literature were used to construct the *in silico E. coli* strain[1,3,12]. We simulated the metabolic capabilities as previously described with the objective of maximizing growth[12,14,21]. Both growth and maintenance requirements were imposed on the *in silico* model[12–14]. The growth experiments were done in M9 minimal medium with the addition of the carbon source. The growth rate was varied by changing the concentration of the carbon source (ranging from 0.25 to 3 $g\,l^{-1}$) and the temperature (ranging from 29 °C to 37 °C). *E. coli* MG1655 (ATCC #47076) was used for all of the experiments.

Batch cultures were set up at two different volume scales. One-litre (large) cultures were performed in 1.5-l Erlenmeyer flasks sparging with air. The large-volume batch cultures were used to continuously monitor the oxygen uptake rate (OUR) online with an off-gas analyser. Small (100–250 ml) cultures were grown in 500–1,000 ml Erlenmeyer flasks. For the small-scale cultures the OUR was monitored online polarographically and by measuring the mass transfer coefficient for oxygen (k_La) (see below). The temperature was controlled by using a circulating water bath (Haake). We measured and analysed data during exponential growth. The biomass and the concentration of the substrate (malate, glucose, glycerol) in the media were monitored throughout the experiment.

Analytical procedures

Cellular growth rate was monitored by measuring the absorbance (A, or optical density) at 600 nm and 420 nm and by cell counts (Coulter Electronics). The doubling time was calculated from the growth rate: $t_d = \ln(2)/\mu$. Absorbance to cellular dry weight correlations were determined by two different measurements: (1) spun-down cells were dried at 75 °C to a constant weight; and (2) 25–50 ml samples (taken throughout the culture) were filtered, washed and dried to a constant weight. The concentration of metabolites in the culture media was determined by high-performance liquid chromatography (HPLC) (Rainin Instruments). An aminex HPX-87H ion exchange carbohydrate–organic acid column (Bio-Rad Laboratories) (65 °C) was used with degassed 5 mM sulphuric acid as the mobile phase and ultraviolet detection. Glucose and glycerol were monitored by enzymatic assay (Sigma). The dissolved oxygen in the culture was monitored with a polarographic dissolved oxygen probe (Cole-Parmer Instruments). Oxygen consumption was measured in three different ways: (1) passing the effluent gas through a Servomex oxygen analyser (model 1140C) (Servomex); (2) calculated from the dissolved oxygen reading and k_La measurements; and (3) in a respirometer chamber in a separate 70-ml flask. All three methods used for measuring the OUR gave similar and reproducible results.

Adaptive evolution

Cultures in prolonged exponential growth were started from individual colonies and were grown in micro-carrier spinner flasks at 250 ml within a temperature-controlled incubator. Serial transfers were made during the exponential phase of growth at mid-log-phase ($A_{600\,nm} = 0.55$) using an adjusted inoculum volume based on the growth rate of the culture. On a daily basis, the growth rate, time of inoculation, $A_{600\,nm}$ of the culture, and any visual changes in the composition of the culture were recorded. Samples of cultures were stored on a daily basis. The culture was tested weekly for pH and phenotyped (by plating) for any signs of coexistence with a distinct population of mutants or foreign contamination. No discernible differences in colony morphology or signs of foreign contamination were observed during these experiments.

Phenotype phase plane analysis

First, the metabolic reconstruction was done using biochemistry, genomic and physiological data[3–5]. Second, mass balance, capacity and thermodynamic constraints were imposed on the network to define a solution space[13]. Third, the best use of the metabolic network for a given objective was identified using linear optimization[16–18]. Fourth, all optimal solutions as a function of two constraints were presented on the PPP[21]. The PPP has distinct phases. Each phase corresponds to a particular type of an optimal solution, which in turn represents a particular flux distribution through the network. Each phase has certain metabolic characteristics; for instance, phase 2 in the figures presented here was characterized by an acetate overflow. The lines that demarcate the phases were defined by changes in the shadow price structure of the optimal solution. The properties of the PPP have been detailed elsewhere[21]. In this study, the optimal utilization of the metabolic network was predicted *a priori*, based on a previously developed *in silico* model[12,14].

Received 12 December 2001; accepted 2 September 2002; doi:10.1038/nature01149.

1. Blattner, F. R. *et al.* The complete genome sequence of *Escherichia coli* K-12. *Science* **277,** 1453–1474 (1997).
2. Drell, D. The Department of Energy Microbial Cell Project: a 180° paradigm shift for biology. *OMICS* **6,** 3–9 (2002).
3. Covert, M. W. *et al.* Metabolic modeling of microbial strains *in silico*. *Trends Biochem. Sci.* **26,** 179–186 (2001).
4. Selkov, E., Maltsev, N., Olsen, G. J., Overbeek, R. & Whitman, W. B. A reconstruction of the metabolism of *Methanococcus jannaschii* from sequence data. *Gene* **197,** GC11–GC26 (1997).
5. Overbeek, R. *et al.* WIT: integrated system for high-throughput genome sequence analysis and metabolic reconstruction. *Nucleic Acids Res.* **28,** 123–125 (2000).
6. Karp, P. D. *et al.* The EcoCyc database. *Nucleic Acids Res.* **30,** 56–58 (2002).
7. Gombert, A. K. & Nielsen, J. Mathematical modelling of metabolism. *Curr. Opin. Biotechnol.* **11,** 180–186 (2000).
8. Tomita, M. *et al.* E-CELL: software environment for whole-cell simulation. *Bioinformatics* **15,** 72–84 (1999).
9. Fell, D. *Understanding the Control of Metabolism* (Portland, London, 1996).
10. Schuster, S., Fell, D. A. & Dandekar, T. A general definition of metabolic pathways useful for systematic organization and analysis of complex metabolic networks. *Nature Biotechnol.* **18,** 326–332 (2000).
11. Schilling, C. H. *et al.* Genome-scale metabolic model of *Helicobacter pylori* 26695. *J. Bacteriol.* **184,** 4582–4593 (2002).
12. Edwards, J. S. & Palsson, B. O. The *Escherichia coli* MG 1655 *in silico* metabolic genotype: its definition, characteristics, and capabilities. *Proc. Natl Acad. Sci. USA* **97,** 5528–5533 (2000).
13. Varma, A. & Palsson, B. O. Stoichiometric flux balance models quantitatively predict growth and metabolic by-product secretion in wild-type *Escherichia coli* W3110. *Appl. Environ. Microbiol.* **60,** 3724–3731 (1994).
14. Edwards, J. S., Ibarra, R. U. & Palsson, B. O. *In silico* predictions of *Escherichia coli* metabolic capabilities are consistent with experimental data. *Nature Biotechnol.* **19,** 125–130 (2001).
15. Palsson, B. O. The challenges of *in silico* biology. *Nature Biotechnol.* **18,** 1147–1150 (2000).
16. Edwards, J. S., Ramakrishna, R., Schilling, C. H. & Palsson, B. O. *Metabolic Engineering* (eds Lee, S. Y. and Papoutsakis, E. T.) (Marcel Dekker, New York, 1999).
17. Bonarius, H. P. J., Schmid, G. & Tramper, J. Flux analysis of underdetermined metabolic networks: The quest for the missing constraints. *Trends Biotechnol.* **15,** 308–314 (1997).
18. Varma, A. & Palsson, B. O. Metabolic flux balancing: basic concepts, scientific and practical use. *Bio/Technology* **12,** 994–998 (1994).
19. Wiechert, W. Modeling and simulation: tools for metabolic engineering. *J. Biotechnol.* **94,** 37–63 (2002).
20. Schilling, C. H., Edwards, J. S., Letscher, D. & Palsson, B. O. Combining pathway analysis with flux balance analysis for the comprehensive study of metabolic systems. *Biotechnol. Bioeng.* **71,** 286–306 (2000).
21. Edwards, J. S., Ramakrishna, R. & Palsson, B. O. Characterizing the metabolic phenotype: a phenotype phase plane analysis. *Biotechnol. Bioeng.* **77,** 27–36 (2002).
22. Weikert, C., Sauer, U. & Bailey, J. E. Use of a glycerol-limited, long-term chemostat for isolation of *Escherichia coli* mutants with improved physiological properties. *Microbiology* **143,** 1567–1574 (1997).

Acknowledgements We thank L. Ramos, J. DiTonno, S. Fong, J. Marciniak, N. Short and H. Bialy for technical assistance and for reviewing the manuscript. We acknowledge funding support from the National Institutes for Health and the National Science Foundation, and the Department of Energy Office of Biological and Environmental Research.

Competing interests statement The authors declare competing financial interests: details accompany the paper on *Nature*'s website (http://www.nature.com/nature).

Correspondence and requests for materials should be addressed to B.Ø.P (e-mail: palsson@ucsd.edu).